communications chemistry

Article

A Nature Portfolio journal

https://doi.org/10.1038/s42004-025-01689-7

# Direct observation and identification of resonance-stabilized radicals in a sooting flame



X. Mercier[1] ✉, J. Bourgalais[2], A. Faccinetto[1], L.-S. Tran[1], J. Elias[1,3], P. Demaux[1], A. Lahccen[1], B. Calimet[1], L. Nahon[4] & G. A. Garcia[4]

Understanding the molecular mechanisms governing soot inception is critical for developing accurate models of particulate formation in combustion systems. Polycyclic aromatic hydrocarbons (PAHs) are well established as key precursors/intermediates that participate to soot formation, but the growth reactions towards the particulate phase are still the subject of active debate. Among the proposed chemical mechanisms, aromatic resonance-stabilized radicals (RSRs) offer a promising alternative pathway, but their in situ detection in flames has proven challenging, limiting further mechanistic insight. Here, we report the direct observation and identification of several polycyclic aromatic RSRs, using a combination of synchrotron-based mass-selected vacuum ultraviolet photoelectron spectroscopy and quantum chemical calculations. The existence of both delocalized and localized π-radicals and their specific implication on the different stages of soot formation, via radical-driven PAH reaction mechanisms, is discussed in the context of combustion chemistry.

Soot formation in combustion processes is a critical phenomenon with wide-ranging implications for environmental sciences, public health, and combustion technology. Soot particles are major contributors to air pollution and climate change[1–4]. These particles exacerbate respiratory and cardiovascular diseases[5] and pose carcinogenic risks[6,7] due to their association with polycyclic aromatic hydrocarbons (PAHs). Beyond terrestrial concerns, understanding soot formation is also relevant for research on interstellar carbon and the origin of carbon grains in space[8]. PAHs are universally recognized as key precursors in soot inception, acting as molecular building blocks in the transition from gas-phase precursors to condensed-phase particles[9,10]. The hydrogen-abstraction/acetylene-addition (HACA) mechanism has historically been the dominant framework for explaining PAH growth in high-temperature environments[11]. However, HACA has limitations, particularly in explaining the formation of complex PAHs[12] and soot in radical-poor conditions where acetylene and H-abstraction sites are scarce.

These limitations have led to growing interest in alternative mechanisms and pathways[13–15] that could contribute to PAH growth and soot inception, particularly mechanisms involving resonance-stabilized radicals (RSRs), radical–radical interactions, and weakly bound molecular clusters[16–31]. RSRs have recently emerged as critical intermediates in soot formation, offering an alternative route to PAH clustering and molecular weight growth that does not rely on acetylene addition.

Johansson et al.[32] notably proposed a soot inception mechanism involving RSRs that initiate a radical chain process, enabling the clustering of both radicals and unsaturated closed-shell species, including PAHs. This pathway, referred to as the clustering of hydrocarbons by radical chain reactions (CHRCR), offers the advantage of allowing particle growth without depleting the radical pool, thus sustaining reactivity during the inception stage. In this context, the pioneering work of Rundel et al.[17] provided early evidence for covalently bound clusters (CBCs) of aromatic RSRs, demonstrating indenyl–indenyl clustering during indene pyrolysis and also indenyl–ethylene clustering when indene was added to ethylene in pyrolysis experiments.

Martin et al.[33] demonstrated the importance of π-radical localization in determining the stability and reactivity of PAHs during soot inception. Their study emphasized the dual nature of radicals: delocalized radicals, such as phenalenyl, facilitate weak multicenter bonding ("pancake bonds"), enabling molecular stacking, while localized radicals contribute to the formation of thermally stable single-center bonds. This interplay between radical localization and reactivity highlights the need to understand the electronic structures of RSRs in soot inception.

[1]Université Lille, CNRS, UMR 8522 - PC2A - Physicochimie des Processus de Combustion et de l'Atmosphère, Lille, France. [2]Univ Rennes, CNRS, IPR (Institut de Physique de Rennes)—UMR 6251, Rennes, France. [3]French Environment and Energy Management Agency, Angers, France. [4]Synchrotron SOLEIL, L'Orme des Merisiers, Gif sur Yvette, France. ✉e-mail: xavier.mercier@univ-lille.fr

The recent works of Frenklach[18] and Mebel et al.[25,34,35] further expanded our understanding by exploring the mechanisms underlying PAH clustering and the formation of E-bridge PAHs. Their theoretical studies highlighted the significance of radical–molecule interactions in the formation of large PAH clusters. They notably proposed that E-bridge PAHs form through chemical pathways primarily governed by an updated HACA mechanism, involving the creation of a rotationally activated dimer via the collision of an aromatic molecule with an aromatic radical. E-bridges were proposed to play a pivotal role in stabilizing molecular clusters during the early stages of soot formation, providing a molecular-level explanation for the transition from isolated PAHs to condensed-phase soot particles.

Advances in experimental techniques, such as electron paramagnetic resonance (EPR) and high-resolution atomic force microscopy (HR-AFM), have also been instrumental in unraveling the complexity of soot inception[22,23,26,36–38]. Notably, Commodo et al.[37] employed HR-AFM to infer the structure of molecular precursors of incipient soot particles, revealing the presence of partially saturated and unsaturated π-radicals. Their work provided evidence for the involvement of these species in molecular clustering and identified structural motifs indicative of π-stacking interactions, further linking RSR behavior to early soot formation.

Pulsed EPR experiments also highlighted highly branched RSRs with aliphatic groups associated with soot inception[31]. Additionally, synchrotron-based photoionization mass spectrometry experiments by Wang et al.[39,40] have identified CBCs of aromatic RSRs in combustion environments, indicating a propensity for clustering and the role of CBCs as key intermediates in the transition from RSRs to PAHs during pyrolysis experiments. Their study also supports the importance of H-abstraction and radical addition in driving cluster formation, as proposed by Johansson et al.[32], where clusters undergo progressive H-loss to yield stable PAHs. This mechanism, termed progressive hydrogen loss from covalently bound clusters (PHLCBC), similarly to the CHRCR mechanism, suggests an intricate interplay between RSRs, CBCs, and PAHs in soot inception.

Despite the recent advances in the development of the theoretical framework and in the improvement of the experimental diagnostics, the unambiguous identification of RSR PAHs has yet to be achieved, and therefore their association with soot inception remains unclear and needs to be established. Currently, the involvement of RSR PAHs in soot inception is a subject of active investigation with ongoing efforts to detect these species in combustion environments using advanced spectroscopic and analytical techniques and to model their formation pathways through quantum chemistry and kinetic simulations. The reactivity of these species is closely linked to their structure, as electron delocalization enhances stability, while steric and electronic effects influence the ability to participate in clustering and molecular growth processes. However, there remain important open questions, notably regarding whether RSR PAHs act as primary soot precursors or transient intermediates, their dominant formation mechanisms, and their precise role in molecular clustering leading to particle inception.

In this context, the present study provides direct experimental identification of specific RSR PAH radicals in the soot inception zone of a diffusion flame. Using synchrotron-based vacuum ultraviolet photoelectron/photoion coincidence spectroscopy (SVUV-PEPICO) combined with quantum chemical simulations, delocalized and localized π-radicals are selectively identified—including phenalenyl, 9-hydroanthracenyl, 7H-benzo[de]anthracenyl, and olympicenyl. This approach provides strong spectroscopic evidence of their presence and offers new insights into their potential roles in non-covalent multicenter bonding and covalent cross-linking.

## Results and discussion

### Isomeric discrimination of RSR PAHs and PAHs

Adiabatic ionization energies (AIEs) of PAHs are well-documented in the literature, particularly for low to moderate-sized PAHs. Notably, the NIST webbook[41] compiles a large database of experimental AIEs determined for such compounds. In Fig. 1, the experimental AIEs of selected PAHs, chosen over the mass range *m*/*z* 100–400, have been reported. These selected PAHs correspond to those used by Bourgalais et al.[42] in a previous study to demonstrate the accuracy of the DFT/M06-2X method for calculating the AIEs of PAHs and related molecules, including RSR PAHs, which are far less documented in the literature. The accuracy of M06-2X is shown to be comparable to that of the "gold standard" coupled cluster CCSD(T)-F12 method, which becomes computationally expensive as the size of the molecular system increases. This high level of accuracy is partly attributed to the significant amount of exact exchange incorporated into the DFT functional, which improves the description of non-local correlation effects. This is particularly beneficial for systems with delocalized electrons, such as PAHs. Building on this work, we used the DFT/M06-2X/6-311+G* method to calculate the AIEs of several RSR PAHs, as reported in Table S1. Part of these RSR PAHs were directly issued from the work of Selvakumar et al.[43] and suggested to be implicated in soot inception. Their calculated AIEs are also shown in Fig. 1.

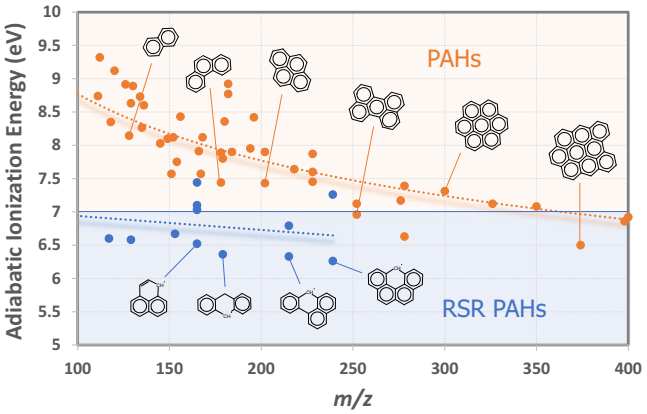


**Fig. 1 | Adiabatic ionization energies comparison for PAHs and RSR PAHs.** AIEs of selected PAHs (orange, experimental values) [44] and RSR PAHs (blue, DFT/M06-2X/6-311+G* calculations from this work). Dotted lines represent power-law (PAHs) and linear fits (RSR PAH) as visual guides. Based on the recent benchmarking study reported in Bourgalais et al.[42], AIE uncertainties from DFT are expected to remain below 0.05 eV.

AIEs of selected PAHs (orange, experimental values)[44] and RSR PAHs (blue, DFT/M06-2X/6-311+G* calculations from this work). Dotted lines represent power-law (PAHs) and linear fits (RSR PAH) as visual guides. Based on the recent benchmarking study reported in Bourgalais et al.[42], AIE uncertainties from DFT are expected to remain below 0.05 eV.

The data representation shows that the AIEs of PAHs and RSR PAHs can be broadly separated into two distinct zones. The first zone, delimited by the orange box in Fig. 1, contains most of the experimental AIEs of the selected aromatic compounds and PAHs compiled in Bourgalais et al.[42]. These PAHs have masses up to *m*/*z* 400 ($C_{32}H_{16}$-dibenzo[a,j]coronene), with AIEs mostly comprised between 7 and 10 eV and following a general trend assimilated to a power-law decrease as the molecular mass of the PAHs increases. This trend is attributed to the stabilization of the ionized state through extensive π-electron delocalization, which becomes more pronounced with larger PAHs. In contrast, the calculated AIEs of the selected RSR PAHs from the work of Selvakumar et al.[43] are essentially contained within a second zone, defined by the blue box in Fig. 1. The graph shows that these AIEs follow a linear trend with respect to the RSR PAH masses, most of them being comprised between 6 and 7 eV. Unlike PAHs, the AIE of RSR PAHs is primarily determined by how well the radical center is conjugated with the rest of the molecule. This results in a weaker dependence on molecular size.

From these data, it appears possible to preferentially ionize and detect RSR PAHs by exploiting the difference in ionization energy between PAHs and RSRs. By carefully setting the ionization energy just slightly above that of the radicals, the PAH contribution to the background and the potential $^{13}C$

contamination (see below) can be avoided, improving the detection of RSRs, which are found in very low concentrations. Such a strategy is made feasible by experimental setups utilizing high-repetition tunable VUV sources, such as synchrotron radiation. Here, we employ this capability in combination with a spectrometer using a PEPICO scheme, enabling a precise identification of the molecular structure of the species by mass-selected photoelectron spectroscopy (ms-PES). We first investigate the impact of the ionization energy on the recorded mass spectra at a fixed sampling height, 55 mm above the burner (HAB), along the central vertical axis of a laminar diffusion methane flame. The selection of this specific HAB relies on previous studies[29–31,38,45] highlighting this region as the beginning of the soot inception zone. This determination was initially made using in situ laser-induced incandescence and later confirmed by ex situ time-of-flight secondary ion mass spectrometry and Raman spectroscopy analyses. Moreover, the presence of RSR PAHs at this specific HAB was previously highlighted by continuous and pulsed EPR experiments[38]. Note that only one set of flame flow conditions was investigated in this study that offer a stable and reproducible environment to probe incipient soot precursors[29,38,45]. However, the variations in fuel composition or flow rates may influence the position and abundance of the RSRs generated in the flame.

Only selected parts of the mass spectra acquired respectively for fixed ionization energies 7, 8, and 9 eV are reported in Fig. 2. We intentionally limited the reported mass range of the spectra between *m/z* 160 and 244 to better highlight the identification of RSR PAHs sampled from the flame. Peak signals corresponding to PAHs and coming from the soot inception zone of the flame were detected up to *m/z* 374 with the PEPICO setup and reported in Fig. S1. From Fig. 2, the mass spectra acquired at 8 and 9 eV are remarkably similar and show a set of mass peaks with comparable relative intensity ratios, characteristic of low- to moderate-sized PAHs formed in the inception zone. All these PAHs have ionization energies between 8 and 9 eV, as reported in Fig. 1. The mass spectra are characterized by peaks at even *m/z* followed by the $^{13}C$ isotopic contributions at M + 1 and M + 2. Because the ionization energies are close to the AIEs, we do not expect nor detect fragment ions, which would be characterized by a broader peak shape due to the kinetic energy released in dissociative ionization processes[46].

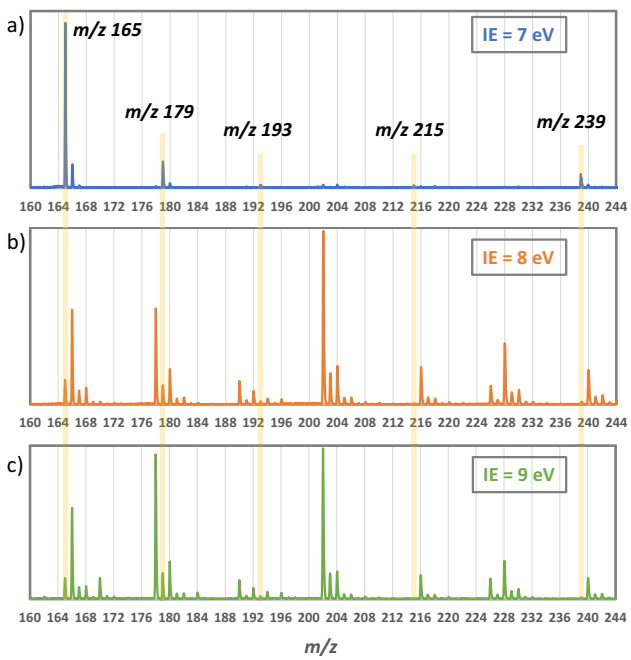


**Fig. 2 | Mass spectra in the soot inception region.** Selected part (*m/z* 160–244) of the mass spectra acquired at different fixed photon energies: (**a**) 7, (**b**) 8, and (**c**) 9 eV in the soot inception region of the flame (55 mm HAB).

Ions resulting from the direct ionization of RSR PAHs are necessarily detected at odd *m/z*. Hence, in the context of combustion chemistry, peak signals of RSR PAHs may overlap with the M + 1 isotopic contribution of PAHs. As the concentration of RSR PAHs is expected to be one or two orders of magnitude lower than that of PAHs, such peak overlap can severely blind and preclude the detection of RSR PAHs. In these conditions, the identification of an RSR PAH appears only possible in the absence of M-1 PAHs. This case corresponds, for instance, to the species detected at *m/z* 165 in Fig. 2 for which no peak signal is detected at *m/z* 164, which therefore strongly suggests the species at *m/z* 165 to be an RSR PAH. However, in the context of sooting flame studies, many different PAHs are formed. By carefully looking at the entire mass spectra recorded at 8 and 9 eV, we could not clearly highlight any other isolated odd *m/z* number, except for *m/z* 239, which may indicate as well the formation of RSR PAHs.

To improve the selectivity of the setup for RSR PAHs detection, it appears therefore interesting to decrease the ionization energy to limit the ionization of PAHs, as shown in Fig. 1. This approach was tested by conducting the experiment at 7 eV ionization energy, with the resulting mass spectrum shown in Fig. 2a. As expected, the mass spectrum recorded at this lower ionization energy is significantly less rich of signals compared to those in Fig. 2b, c. Most of the peaks characteristic of PAHs appearing on these two mass spectra vanish in Fig. 2a, and only a few isolated peaks at odd *m/z* are clearly visible, such as *m/z* 165, 179, 193, 215, and 239. These *m/z* are all consistent with molecular masses of RSR PAHs suggested by Selvakumar et al.[43], based on a density functional theory study, to be involved in soot formation, except for *m/z* 193, which was not identified. The assignment of the species at *m/z* 193 remains, therefore, tentative. While RSR candidates related to the formation of adducts, such as between indenyl and benzene, were considered, the limited resolution and signal-to-noise ratio at this *m/z* preclude its clear identification and no definitive assignments can be based on this data.

For the other masses, we report in Fig. 3 the chemical structures of the RSR PAH candidates discussed in the work of Selvakumar et al.[43] that might correspond to these peaks. As can be seen, several isomers exist for most of these RSR PAHs, which cannot be pinpointed using the mass spectrum alone.

### RSR PAH identification from the experimental ms-PES

As described in the "Methods", the PEPICO setup enables the simultaneous recording of the mass spectrum and the electron spectrum, leading to ms-PES. PES represents a unique spectral fingerprint of the ionized species, as each transition from the ground state of the neutral into the vibronic state of the cation corresponds to a given kinetic energy of the emitted electrons. This makes the PEPICO setup a powerful tool for selectively detecting isomers based on their distinct vibrational structures[47]. However, this identification requires the knowledge of reference PES of pure species or, at least, the AIEs of the expected species for a specific mass[48]. While a large amount of experimental PES and AIEs is available for PAHs in the literature, and much of it can be accessed directly from the webbook NIST database[41], such crucial information for RSR PAHs remains scarce. To compensate for this lack of data, we used the benchmark work of the DFT/M06-2X method by Bourgalais et al.[42] to build up the RSR PAH AIE database reported in Table S1. Note that a large part of the species in this database are chosen from the RSR PAHs suggested to participate in soot formation mechanisms, as discussed in Selvakumar et al.[43], and whose masses match our experimental observations.

We report in Fig. 4 the experimental PES of *m/z* 165, 179, 215, and 239 (red lines), alongside the Frank Condon factors (FCF) calculated at 0 K for the RSR PAHs listed in Table S1. The FCFs represent the overlap integrals of the wavefunctions for vibronic transitions between the neutral and cationic ground states and are expected to be strong for the 0–0 transition of RSR PAHs, which aligns closely with their AIEs. This behavior is attributed to the relatively weak Jahn–Teller effect observed for PAHs, which minimizes structural deformation upon photoionization due to their rigid skeleton[49]. Consequently, the ionization process remains well within the

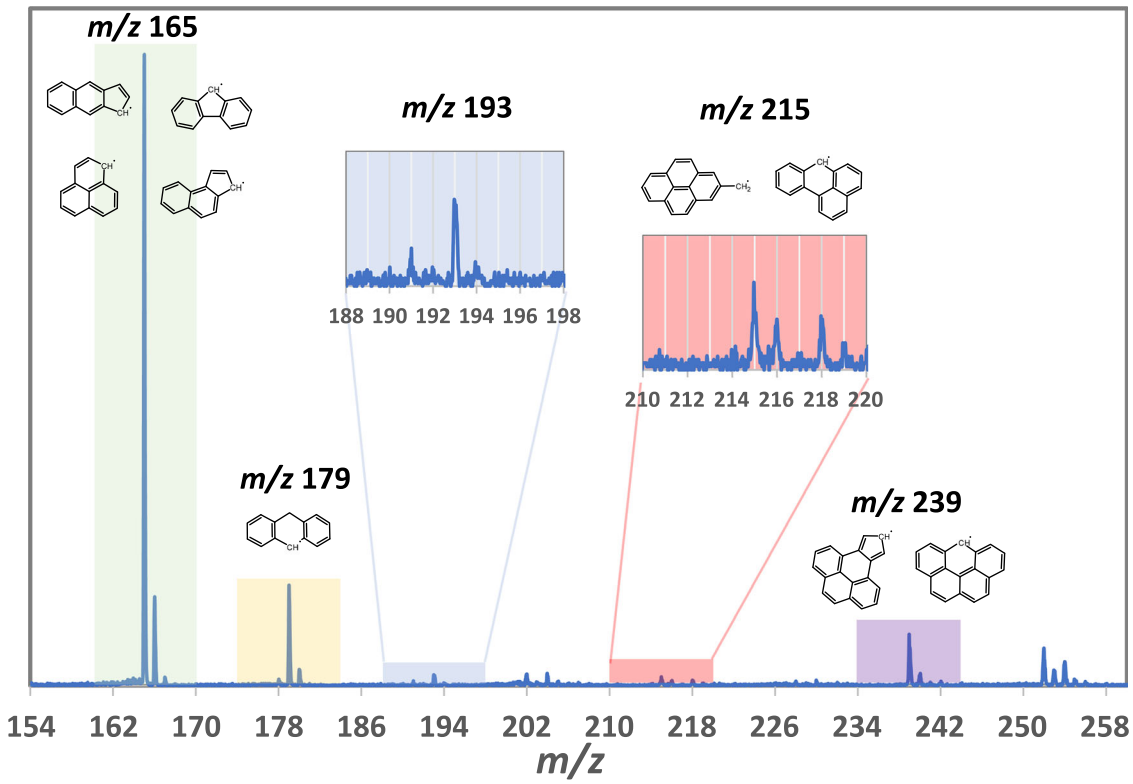


**Fig. 3 | Candidate RSR PAHs are consistent with mass spectral signals.** Candidates RSR PAHs based on Selvakumar et al.[43] consistent with the signals detected at 55 mm HAB.

Franck–Condon region, producing sharp first transitions and well-defined simulated spectra. These calculations provide a reliable reference for comparison with the experimental PES, as confirmed by the excellent match between the position of the first peak in each experimental PES and the 0–0 transition for all four *m/z* values shown in Fig. 4. However, as mentioned in the "Methods" section, the temperature limitation of the simulations, combined with the low signal-to-noise ratio of the experimental spectra, make the identification of additional minor isomers within each mass channel challenging. Therefore, some of the assignments proposed in this work are intended as suggestions, based on the current understanding of the underlying soot chemistry.

The calculated stick spectrum was then combined with a Gaussian profile featuring an arbitrary 200 $cm^{-1}$ bandwidth. We identify with good level of confidence the four main RSR PAHs associated with the *m/z* 165, 179, 215, and 239 mass peaks as phenalenyl (*m/z* 165, $C_{13}H_9$), 9-hydroanthracenyl (*m/z* 179, $C_{14}H_{11}$), 7H-benzo[de]anthracenyl (*m/z* 215, $C_{17}H_{11}$), and 6H-benzo[cd]pyrenyl (*m/z* 239, $C_{19}H_{11}$) more commonly known as olympicenyl. The molecular formulae and structures of these RSR PAHs are reported in the corresponding figures.

Concerning the *m/z* 165 PES, these data can be further completed by the PES obtained at 8 eV reported in Fig. 5 because of the absence of overlap with the isotopic $M+1$ of PAH at *m/z* 164. In that case, the PES recorded at this ionization energy confirms the absence of the three other possible RSR PAHs—fluorenyl, benz[e]indenyl, and benz[f]indenyl—characterized by higher AIEs, respectively calculated at 7.10, 7.44, and 7.03 eV in this work. However, the PES does corroborate the presence of a peak at 6.7 eV, which cannot be attributed to transitions to electronically excited states of the phenalenyl cation. Assuming the FC simulation is correct, the signal would correspond to another isomer, which could be 1-methylacenapthylenyl, for which we calculate an AIE of 6.75 eV. The calculated FCFs, although not matching exactly the experimental peak around 6.7 eV in Figs. 4 and 5, appear very close to this spectral feature. Methylacenapthylenyl, although its identification remains more speculative, has been proposed in the literature as a major intermediate species leading to the formation of the phenalenyl radical from acenaphthylene, according to a CH cycloaddition mechanism converting five-member rings to six-member rings[50]. In their work, the authors mentioned that such a ring expansion mechanism "*could account for the formation of PAHs beyond the phenalenyl radical, such as pyrene, cyclopenta[cd]pyrene, and the olympicenyl radical*". The detection of these compounds as well as methylacenapthylenyl in our work therefore supports this hypothesis of the CH cycloaddition mechanism as a plausible explanation for PAHs growth in flames in conjunction to the main dominant HACA mechanism.

The comparison of the simulated PES of 9-hydroanthracenyl with the experimentally determined PES at *m/z* 179 also provides very good agreement with the first peak around 6.4 eV. However, it is also possible that another minor isomer peaking around 6.55 eV forms at this mass.

The signal recorded at *m/z* 215 exhibits a very good agreement with the calculated FCFs, clearly pointing to the formation of 7H-benzo[de] anthracenyl. As can be deduced from the error bars characterizing the experimental spectrum, the signal recorded for this mass is rather weak and noisy. However, it does not seem that another major isomeric species is present at this mass. Note that calculations on excited states have been performed, indicating that they are not accessible within this energy range, ruling out their possible contribution.

Finally, the plot of the calculated FCFs and recorded spectrum at *m/z* 239 clearly demonstrates the formation of olympicenyl, characterized by an AIE of 6.26 eV. The low signal-to-noise ratio of the experimental spectrum and the relatively noisy signal above 6.5 eV hinder further discussion on other structures with spectral features peaking between 6.5 and 7 eV. As for the *m/z* 165 PES, the analysis of the *m/z* 239 obtained at 7 eV can be completed using the PES recorded at 8 eV reported in Fig. 5. Despite the low signal-to-noise ratio, this PES clearly points to the existence of another peak around 7.05 eV, which has been identified as 4H-cyclopenta[def]triphenylene. This species, not discussed in the paper of Selvakumar et al.[43],

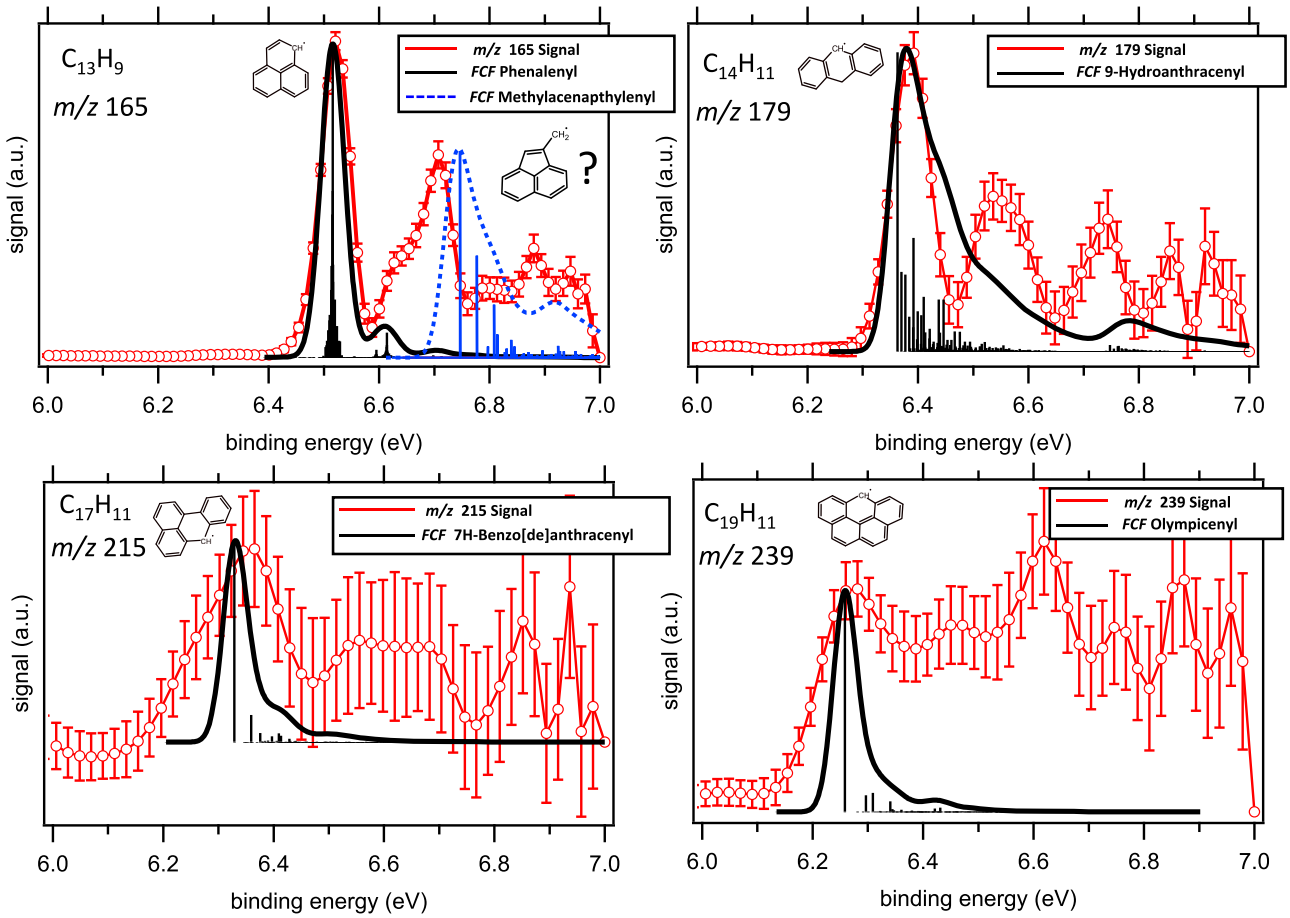


**Fig. 4 | Photoelectron spectra obtained at 7 eV.** PES of *m/z* 165, 179, 215, and 239 signals recorded at 55 mm HAB in the flame obtained at 7 eV. Comparison with calculated FCF spectra of RSR PAHs.

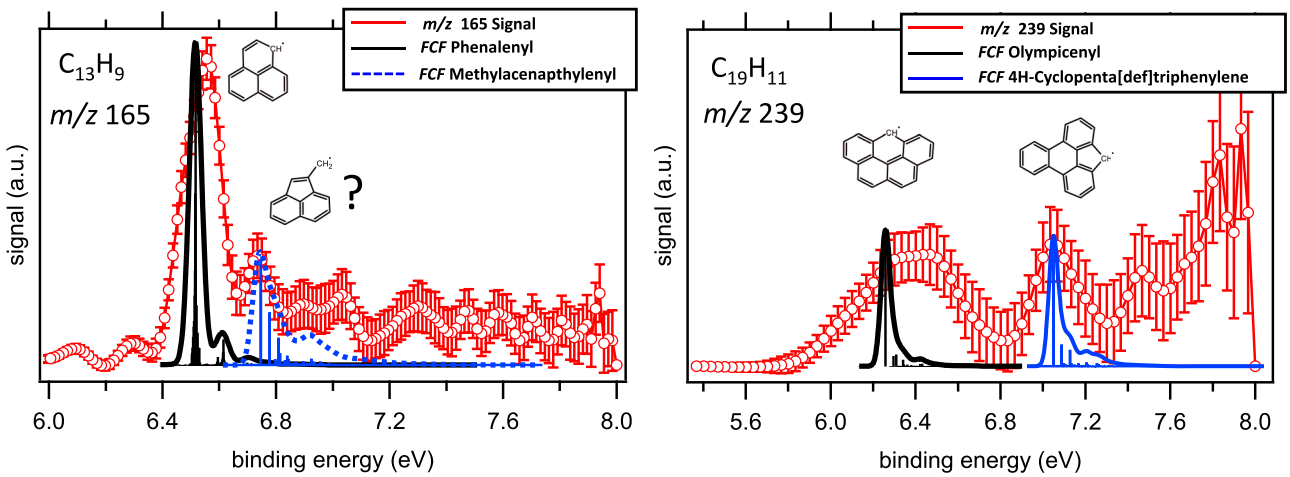


**Fig. 5 | Photoelectron spectra obtained at 8 eV.** PES of *m/z* 165 and 239 signals recorded at 55 mm HAB in the flame obtained at 8 eV. Comparison with calculated FCF spectra of RSR PAHs.

belongs to the family of the fluorenyl type compounds according to their classification.

### Implications for soot formation mechanisms

The analysis of the PES indicates the formation of π-radicals in the soot inception zone, corroborating previous studies that suggested the participation of such species in soot formation processes[22,25,30,31,33–36,38,43,45]. As discussed in detail by Selvakumar et al.[43], these radicals can be classified according to their degree of localization, as assessed through DFT calculations and Mulliken spin populations. This methodology provides a reactivity indicator, ranging from 0 to 1, defining the propensity of π-radicals to form bonds with other aromatic molecules[33,43]. The identified RSR species in our experiments exhibit varying degrees of π-radical localization, as determined through this classification system. Phenalenyl (*m/z* 165, $C_{13}H_9$) with a Mulliken spin population of 0.30, belongs to the class of delocalized π-radicals, whereas 7H-benzo[de]anthracenyl (*m/z* 215, $C_{17}H_{11}$) and

olympicenyl (*m*/*z* 239, $C_{19}H_{11}$), both characterized by Mulliken spin populations of 0.46, are defined as weakly localized π-radicals. Finally, 9-hydroanthracenyl (*m*/*z* 179, $C_{14}H_{11}$) with a Mulliken spin population of 0.62 is classified as a strongly localized π-radical. 4H-cyclopenta[def]triphenylene (*m*/*z* 239, $C_{19}H_{11}$) has not been classified by Selvakumar et al.[43], but as a fluorenyl type species, it should be characterized by a Mulliken spin population around 0.60, belonging therefore to the class of strongly localized π-radicals.

Delocalized π-radicals as phenalenyl have been shown to facilitate the formation of multicenter bonds, such as the two-center/two-electron (2c/2e$^-$) bonds described in prior studies[22,43], which stabilize incipient molecular clusters and support their transition into stable clusters within the flame environment. The delocalized nature of π-radicals is prone to forming multicenter "pancake bonds," theorized as transient stabilization structures in incipient soot particles. π-radical delocalization facilitates molecular stacking, increasing the probability of π–π coupling and eventual soot particle formation[43]. These bonds allow weak, flexible interactions that enable molecular clustering without immediate chemical bonding[51,52] that are crucial for the early steps of soot formation. The identified unsaturated radicals in our study—phenalenyl, 7H-benzo[de]anthracenyl, and olympicenyl—are consistent with this hypothesis. The strong correspondence between the experimental and theoretical PES for these radicals suggests that these species could act as molecular scaffolds for soot inception. Moreover, the low AIEs of these RSR species correlate with increased electronic delocalization, which enhances the likelihood of intermolecular interactions, such as π–π stacking as previously suggested[22,43]. This hypothesis is consistent with the fluorescence excimer signals detected in prior studies[29,45], which may be attributed to transient stacking interactions of the species constituting the core of incipient soot particles.

The 2c/2e$^-$ bonds hypothesis suggested by the nature of the detected species in this work also aligns with previous work by Faccinetto et al.[30], who analyzed mass spectra from the same flame studied here. Their findings highlighted evidence of covalent dimerization of aromatic species with mass comprised between *m*/*z* 152 and 252, bound together by 1, 2, 3, or 4 C–C bonds, with two covalent bonds being the most favorable case. These dimers, stabilized by multicenter bonding, are proposed as precursors for larger soot nuclei. Similarly, theoretical studies by Frenklach and Mebel[18,34,35] show that E-bridge PAHs may play a critical role in stabilizing molecular aggregates. They notably highlighted, from the analysis of potential energy surfaces, the formation of E-bridge dimers from the addition of aceanthrylene to the 1- and 9-anthracenyl radicals. Our detection of 9-hydroanthracenyl, but also larger derivative species such as 7H-benzo[de]anthracenyl and olympicenyl, provides direct experimental evidence supporting these theoretical frameworks. The intermediate localization in 7h-benzo[de]anthracenyl and olympicenyl suggests a dual role: enabling weak stacking interactions and the formation of covalent bridges under specific conditions. These radicals may serve as transitional species, bridging the gap between purely delocalized radicals and strongly localized radicals.

Strongly localized radicals, such as 9-hydroanthracenyl or 4H-cyclopenta[def]triphenylene, have greater thermal stability, as suggested in computational studies[33], enabling them to persist in high-temperature conditions, and to initiate covalent cross-links or bridge structures critical for soot inception. While our data predominantly identify unsaturated π-radicals, the detection of partially saturated radicals as 9-hydroanthracenyl requires further discussion. Partially saturated π-radicals, as observed in HR-AFM studies[23,24], may represent intermediate states between gas-phase PAHs and surface-stabilized radicals involved in soot growth. These strongly localized π-radicals are characterized by their ability to form robust single-center bonds, contributing significantly to the structural stabilization of soot precursors in high-temperature environments. Theoretical and experimental studies have shown that such radicals are less likely to engage in π–π stacking but are critical in creating covalent cross-links within growing molecular aggregates[18,30,34].

Hence, one potential mechanism for molecular aggregation into a soot particle might involve a sequential process of radical addition and stabilization as reported in Fig. 6. The coexistence of delocalized, weakly localized, and strongly localized π radicals highlights the interplay driving molecular weight growth during soot inception. Delocalized radicals, by forming multicenter bonds, may act as intermediates, facilitating the transition between small PAHs, loosely bound molecular clusters, and more stable covalently bonded soot precursors, acting as molecular "glue" for incipient PAH clusters. Weakly localized radicals stabilize these clusters through secondary bonding interactions, while strongly localized radicals, in turn, solidify the structure of these aggregates, enabling their persistence in high-

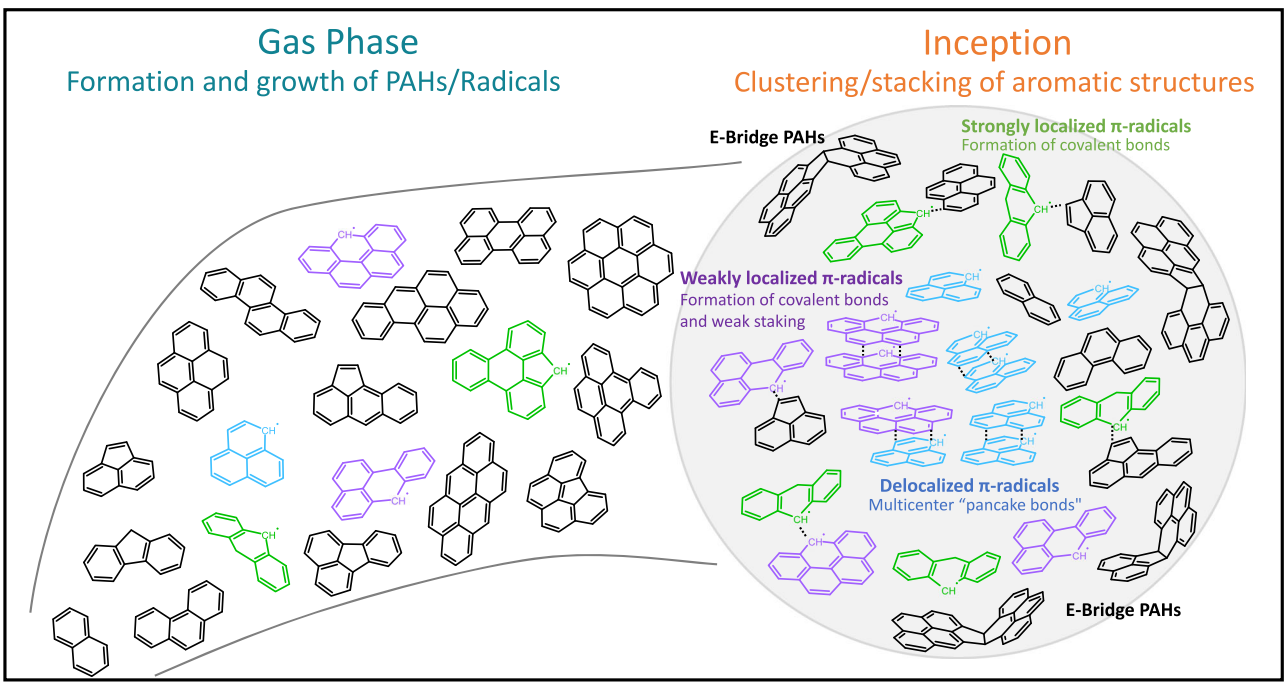


**Fig. 6 | Illustrative soot inception pathways.** Schematic illustration of possible soot particle inception pathways, tentatively highlighting the potential roles of RSRs, CBCs, and PAHs in early particle formation.

temperature environments. This hierarchical mechanism provides a plausible explanation for the molecular diversity observed in the inception zone as illustrated in Fig. 6.

## Conclusions

Through a combined theoretical and experimental study, we demonstrate the in situ formation of phenalenyl ($C_{13}H_9$), 9-hydroanthracenyl ($C_{14}H_{11}$), 7H-benzo[de]anthracenyl ($C_{17}H_{11}$), olympicenyl ($C_{19}H_{11}$), and 4H-cyclopenta[def]triphenylene ($C_{19}H_{11}$) during the early stages of soot formation, highlighting the involvement of both delocalized and localized π radicals.

Delocalized π radicals are suggested to dominate the initial clustering of small PAHs during the inception process, as their electronic configurations are better suited for noncovalent and multicenter bonding. In contrast, weakly or strongly localized radicals, with their higher spin populations and distinct reactivity profiles, should primarily contribute to covalent cross-linking during later stages of soot inception. The experimental and theoretical findings presented in this study strongly support the hypothesis that π-radicals play a central role in soot inception. By identifying key RSR species such as phenalenyl, olympicenyl, and 7H-benzo[de]anthracenyl in the inception region of the flame, this work suggests their unique contributions to early soot formation via mechanisms involving weak stacking interactions and the formation of covalent bridges under specific conditions.

However, while this study provides experimental proof for understanding radical-driven soot inception, several challenges remain. The detection and characterization of partially saturated radicals need to be expanded to the entire flame axis, possibly to include more radicals pertinent to the validation of soot inception models. These species may represent transient intermediates that are either too reactive to persist during the sampling or whose concentration is too low to allow reliable detection or identification. Moreover, the inability to detect certain key radicals, such as the $C_9H_7$ indenyl-type radical, suggests that some species might be too reactive to survive the sampling process or are present in concentrations below the detection threshold. Alternatively, their absence could reflect intrinsic selectivity in the chemical environment, favoring the formation of more stable species. Future studies exploring the entire flame height, using advanced sampling techniques and improved detection sensitivity, may shed more light on the roles of these transient and elusive species.

Beyond combustion science, the findings have broader implications for materials science and astrochemistry, impacting the design of carbon-based nanomaterials and offering clues on the formation of interstellar PAHs.

## Methods

### Experimental methods

This study has been carried out on a 120 mm-high, non-smoking laminar diffusion methane flame (0.52 L $min^{-1}$ $CH_4$, 87 L $min^{-1}$ air) stabilized on a Gülder-type burner at atmospheric pressure already described in detail elsewhere[53,54]. The flame was sampled at 55 mm HAB, corresponding to the onset of soot inception as identified in previous studies using in situ LII[29] and excitation emission matrices fluorescence[45], and ex situ mass spectrometry[30,31].

Chemical species were extracted from the flame using a dilutive quartz microprobe with a 250 µm orifice, connected to the expansion chamber of SAPHIRS[55], where they were ionized by synchrotron radiation. A supplementary flow of He was used to dilute and transport the sampled species to the nozzle expansion. To prevent condensation of high-mass species during transport, notably large PAHs and RSR PAHs, the sampling line was heated and maintained at 400 °C up to the expansion nozzle. This beam expanded through two consecutive skimmers before reaching the SAPHIRS ionization chamber. The undulator-based beamline DESIRS[56] at the French synchrotron center SOLEIL was configured to deliver ~$10^{13}$ photons $s^{-1}$ with an energy resolution of 17 meV, while a pressure of 0.14 mbar of Kr was maintained in the gas filter to ensure spectral purity in the selected energy range by suppressing high-harmonic radiation from the undulator. A simplified schematic of the SVUV-PEPICO setup is reported in Fig. S2.

The DELICIOUS3 double imaging photoelectron/photoion coincidence ($i^2$PEPICO) spectrometer[57], combining a velocity map imaging (VMI) spectrometer to a modified Wiley-McLaren mass spectrometer, was used to obtain mass spectra and mass-selected photoelectron images at fixed photon energies (7, 8, and 9 eV). The VMI-photoelectron images were treated using the pBasex Abel transform algorithm[58] to extract the mass-selected photoelectron spectra. Prior to inversion, the original 1500 × 1500 images were reduced in size to increase the pixel statistics to appropriate levels, as given by the error bars calculated via a Monte Carlo simulation, which assumed a Poisson distribution for each individual pixel. The size was reduced by ×5, ×6, ×8, ×8 for *m/z* 165, 179, 215, and 239, respectively. The raw photoelectron images after size reduction have been compiled in Fig. S3.

### Computational methods

All electronic structure and energy computations in this study were conducted using the Gaussian 09 suite[59] of ab initio programs. Full geometry optimizations of both neutral and cationic species were performed at the DFT/M06-2X/6-311+G* level of theory, with the optimized structure of the neutral species used as the starting point for the corresponding cationic forms. Zero-point energy corrections and vibrational frequency calculations were also performed at the same level of theory to compute the AIEs. The calculated AIEs, presented in Table S1, have not been scaled or adjusted in any way. Notably, a recent benchmarking study reported in Bourgalais et al.[42] estimated the uncertainty of AIEs for PAHs and related compounds computed with this DFT method to be below 0.05 eV.

The simulation of FCFs was carried out using the TI-AH|FC model[60], employing the adiabatic Hessian approach for the electronic transition and the Franck-Condon approximation for transition properties. The computed stick spectrum was obtained by calculating the intensity of each transition between the vibrational initial and final states individually, corresponding to the sum-over-states or time-independent approach. The 0−0 transition was aligned with the calculated AIE.

It is worth noting that, due to the large size of the molecules, temperature effects were not included in the calculations; simulations were therefore performed at 0 K. As a result, hot bands, arising from transitions involving thermally populated vibrational states, are not accounted for. While this limitation may lead to discrepancies beyond the fundamental transitions when comparing with experimental spectra, it is important to emphasize that the accurate prediction of hot bands remains particularly challenging for large molecules such as PAHs and RSR PAHs. This difficulty stems from limitations such as the harmonic approximation and vibronic coupling. Notably, the most intense hot bands often involve low-frequency vibrational modes, which are especially difficult to model accurately within the harmonic Franck–Condon approximation.

## Data availability

The datasets generated during and/or analysed during the current study are available from the corresponding author on reasonable request.

Received: 23 May 2025; Accepted: 3 September 2025;
Published online: 06 October 2025

## References

1. Bond, T. & Bergstrom, R. Light absorption by carbonaceous particles: an investigative review. *Aerosol Sci. Technol.* **40**, 27–67 (2006).
2. Kim, K.-H., Jahan, S. A. & Kabir, E. A review of diseases associated with household air pollution due to the use of biomass fuels. *J. Hazard. Mater.* **192**, 425–431 (2011).
3. Bond, T. C. et al. Bounding the role of black carbon in the climate system: a scientific assessment. *J. Geophys. Res. Atmos.* **118**, 5380–5552 (2013).
4. Service, R. F. Study fingers soot as a major player in global warming. *Science* **319**, 1745–1745 (2008).
5. Chow, J. C. Health effects of fine particulate air pollution: lines that connect. *J. Air Waste Manag. Assoc.* **56**, 707–708 (2006).

6. Petry, T., Schmid, P. & Schlatter, C. The use of toxic equivalency factors in assessing occupational and environmental health risk associated with exposure to airborne mixtures of polycyclic aromatic hydrocarbons (PAHs). *Chemosphere* **32**, 639–648 (1996).
7. Niranjan, R. & Thakur, A. K. The toxicological mechanisms of environmental soot (Black Carbon) and carbon black: focus on oxidative stress and inflammatory pathways. *Front. Immunol.* **8**, 763 (2017).
8. Tielens, A. G. G. M. Interstellar polycyclic aromatic hydrocarbon molecules. *Annu. Rev. Astron. Astrophys.* **46**, 289–337 (2008).
9. Martin, J. W., Salamanca, M. & Kraft, M. Soot inception: carbonaceous nanoparticle formation in flames. *Prog. Energy Combust. Sci.* **88**, 100956 (2022).
10. Wang, H. Formation of nascent soot and other condensed-phase materials in flames. *Proc. Combust. Inst.* **33**, 41–67 (2011).
11. Frenklach, M. & Wang, H. Detailed modeling of soot particle nucleation and growth. *Symp. (Int.) Combust.* **23**, 1559–1566 (1991).
12. Schenk, M. et al. PAH formation and soot morphology in flames of C4 fuels. *Proc. Combust. Inst.* **35**, 1761–1769 (2015).
13. Kaiser, R. I. & Hansen, N. An aromatic Universe–a physical chemistry perspective. *J. Phys. Chem. A* **125**, 3826–3840 (2021).
14. Zhao, L. et al. Molecular mass growth through ring expansion in polycyclic aromatic hydrocarbons via radical–radical reactions. *Nat. Commun.* **10**, 3689 (2019).
15. Couch, D. E., Marchi, M. M. S. & Hansen, N. Experimental observation of molecular-weight growth by the reactions of o-benzyne with benzyl radicals. *Phys. Chem. Chem. Phys.* **26**, 24833–24840 (2024).
16. Michelsen, H. A. Probing soot formation, chemical and physical evolution, and oxidation: a review of in situ diagnostic techniques and needs. *Proc. Combust. Inst.* **36**, 717–735 (2017).
17. Rundel, J. A. et al. Promotion of particle formation by resonance-stabilized radicals during hydrocarbon pyrolysis. *Combust. Flame* **243**, 111942 (2022).
18. Frenklach, M. & Mebel, A. M. On the mechanism of soot nucleation. *Phys. Chem. Chem. Phys.* **22**, 5314–5331 (2020).
19. Kholghy, M. R., Kelesidis, G. A. & Pratsinis, S. E. Reactive polycyclic aromatic hydrocarbon dimerization drives soot nucleation. *Phys. Chem. Chem. Phys.* **20**, 10926–10938 (2018).
20. Eaves, N. A., Dworkin, S. B. & Thomson, M. J. The importance of reversibility in modeling soot nucleation and condensation processes. *Proc. Combust. Inst.* **35**, 1787–1794 (2015).
21. Thomson, M. & Mitra, T. A radical approach to soot formation. *Science* **361**, 978–979 (2018).
22. Vitiello, G. et al. Role of radicals in carbon clustering and soot inception: A combined EPR and Raman spectroscopic study. *Combust. Flame* **205**, 286–294 (2019).
23. Commodo, M., D'Anna, A., De Falco, G., Larciprete, R. & Minutolo, P. Illuminating the earliest stages of the soot formation by photoemission and Raman spectroscopy. *Combust. Flame* **181**, 188–197 (2017).
24. Schulz, F. et al. Insights into incipient soot formation by atomic force microscopy. *Proc. Combust. Inst.* **37**, 885–892 (2019).
25. Savchenkova, A. S. et al. Mechanism of E-bridge formation by various PAH molecules: a theoretical study. *Chem. Phys. Lett.* **799**, 139637 (2022).
26. Liu, P. et al. Rapid soot inception via α-alkynyl substitution of polycyclic aromatic hydrocarbons. *Fuel* **295**, 120580 (2021).
27. Cain, J. P., Camacho, J., Phares, D. J., Wang, H. & Laskin, A. Evidence of aliphatics in nascent soot particles in premixed ethylene flames. *Proc. Comb. Inst.* **33**, 533–540 (2011).
28. Adamson, B. D., Skeen, S. A., Ahmed, M. & Hansen, N. Detection of aliphatically bridged multi-core polycyclic aromatic hydrocarbons in sooting flames with atmospheric-sampling high-resolution tandem mass spectrometry. *J. Phys. Chem. A* **122**, 9338–9349 (2018).
29. Mercier, X., Carrivain, O., Irimiea, C., Faccinetto, A. & Therssen, E. Dimers of polycyclic aromatic hydrocarbons: the missing pieces in the soot formation process. *Phys. Chem. Chem. Phys.* **21**, 8282–8294 (2019).
30. Faccinetto, A. et al. Evidence on the formation of dimers of polycyclic aromatic hydrocarbons in a laminar diffusion flame. *Commun. Chem.* **3**, 1–8 (2020).
31. Elias, J. et al. On the chemical composition and structure of incipient soot in a laminar diffusion flame. *Fuel* **373**, 132056 (2024).
32. Johansson, K. O., Head-Gordon, M. P., Schrader, P. E., Wilson, K. R. & Michelsen, H. A. Resonance-stabilized hydrocarbon-radical chain reactions may explain soot inception and growth. *Science* **361**, 997–1000 (2018).
33. Martin, J. W. et al. Reactivity of polycyclic aromatic hydrocarbon soot precursors: implications of localized π-radicals on rim-based pentagonal rings. *J. Phys. Chem. C.* **123**, 26673–26682 (2019).
34. Semenikhin, A. S. et al. On the mechanism of soot nucleation. II. E-bridge formation at the PAH bay. *Phys. Chem. Chem. Phys.* **22**, 17196–17204 (2020).
35. Frenklach, M., Jasper, A. W. & Mebel, A. M. Phenalenyl growth reactions and implications for prenucleation chemistry of aromatics in flames. *Phys. Chem. Chem. Phys.* **26**, 13034–13048 (2024).
36. Commodo, M. et al. Radicals in nascent soot from laminar premixed ethylene and ehtylene-benzene flames by electron paramagnetic resonance spectroscopy. *Proc. Combust. Inst.* **38**, 1487–1495 (2021).
37. Commodo, M. et al. On the early stages of soot formation: molecular structure elucidation by high-resolution atomic force microscopy. *Combust. Flame* **205**, 154–164 (2019).
38. Elias, J., Faccinetto, A., Vezin, H. & Mercier, X. Investigation of resonance-stabilized radicals associated with soot particle inception using advanced electron paramagnetic resonance techniques. *Commun. Chem.* **6**, 1–9 (2023).
39. Wang, H. et al. Direct observation of covalently bound clusters in resonantly stabilized radical reactions and implications for carbonaceous particle growth. *J. Am. Chem. Soc*. https://doi.org/10.1021/jacs.4c03417 (2024).
40. Wang, H. et al. Resonance-stabilized radical clustering bridges the gap between gaseous precursors and soot in the inception stage. *Proc. Natl. Acad. Sci. USA***122**, e2503292122 (2025).
41. Linstrom, P. J., Mallard, W. G. & Eds. NIST Chemistry WebBook, NIST Standard Reference Database Number 69, (National Institute of Standards and Technology, 2025) 20899, https://doi.org/10.18434/T4D303.
42. Bourgalais, J., Mercier, X., Al-Mogren, M. M. & Hochlaf, M. Accurate prediction of adiabatic ionization energies for PAHs and substituted analogues. *J. Phys. Chem. A* **127**, 8447–8458 (2023).
43. Selvakumar, P. K., Martin, J. W., Lorenzo, M. D., Paskevicius, M. & Buckley, C. E. Role of π-radical localization on thermally stable cross-links between polycyclic aromatic hydrocarbons. *J. Phys. Chem. A* **127**, 6945–6952 (2023).
44. Burgess, D. R. Thermochemical data *in NIST Chemistry WebBook, NIST Standard Reference Database Number 69* (eds. Linstrom, P.J. & Mallard, W.G.) 20899 (National Institute of Standards and Technology, 2025). http://webbook.nist.gov.
45. Elias, J. et al. Advanced characterization of soot precursors via excitation emission matrices fluorescence spectroscopy and molecular modeling. *Carbon* **228**, 119355 (2024).
46. Battin-Leclerc, F. et al. Chemistry deriving from OOQOOH radicals in alkane low-temperature oxidation: a first combined theoretical and electron-ion coincidence mass spectrometry study. *Proc. Combust. Inst.* **38**, 309–319 (2021).
47. Fischer, I. & Pratt, S. T. Photoelectron spectroscopy in molecular physical chemistry. *Phys. Chem. Chem. Phys.* **24**, 1944–1959 (2022).
48. Mercier, X. et al. Selective identification of cyclopentaring-fused PAHs and side-substituted PAHs in a low pressure premixed sooting flame by photoelectron photoion coincidence spectroscopy. *Phys. Chem. Chem. Phys.* **22**, 15926–15944 (2020).

49. Jahn, H. A., Teller, E. & Donnan, F. G. Stability of polyatomic molecules in degenerate electronic states - I—orbital degeneracy. *Proc. R. Soc. A* **161**, 220–235 (1997).
50. Levey, Z. D. et al. PAH growth in flames and space: formation of the phenalenyl radical. *J. Phys. Chem. A* **126**, 101–108 (2022).
51. Xiang, Q. et al. Stable olympicenyl radicals and their π-dimers. *J. Am. Chem. Soc.* **142**, 11022–11031 (2020).
52. Ahmed, J. & Mandal, S. K. Phenalenyl radical: smallest polycyclic odd alternant hydrocarbon present in the graphene sheet. *Chem. Rev.* **122**, 11369–11431 (2022).
53. Elias, J. et al. Thermocouple-based thermometry for laminar sooting flames: Implementation of a fast and simple methodology. *Int. J. Therm. Sci.* **184**, 107973 (2023).
54. Irimiea, C. et al. A comprehensive protocol for chemical analysis of flame combustion emissions by secondary ion mass spectrometry. *Rapid Commun. Mass Spectrom.* **32**, 1015–1025 (2018).
55. Tang, X., Garcia, G. A., Gil, J.-F. & Nahon, L. Vacuum upgrade and enhanced performances of the double imaging electron/ion coincidence end-station at the vacuum ultraviolet beamline DESIRS. *Rev. Sci. Instrum.* **86**, 123108 (2015).
56. Nahon, L. et al. DESIRS: a state-of-the-art VUV beamline featuring high resolution and variable polarization for spectroscopy and dichroism at SOLEIL. *J. Synchrotron Rad.* **19**, 508–520 (2012).
57. Garcia, G. A., Cunha de Miranda, B. K., Tia, M., Daly, S. & Nahon, L. DELICIOUS III: a multipurpose double imaging particle coincidence spectrometer for gas phase vacuum ultraviolet photodynamics studies. *Rev. Sci. Instrum.* **84**, 053112 (2013).
58. Garcia, G. A., Nahon, L. & Powis, I. Two-dimensional charged particle image inversion using a polar basis function expansion. *Rev. Sci. Instrum.* **75**, 4989–4996 (2004).
59. Frisch, M. J. et al. Gaussian 09, Rev. D.01; 2013. *Gaussian 09, Rev. D.01;*2013.
60. Bloino, J., Baiardi, A. & Biczysko, M. Aiming at an accurate prediction of vibrational and electronic spectra for medium-to-large molecules: an overview. *Int. J. Quantum Chem.* **116**, 1543–1574 (2016).


## Acknowledgements

The authors acknowledge SOLEIL for provision of synchrotron radiation under project 20220265. This work was performed using HPC resources from the EXPLOR centre hosted by the University of Lorraine (Project: 2021EXTXX2356). This work was supported by the Agence Nationale de la Recherche through the LABEX CAPPA (ANR-11-LABX-0005), the Agence de l'Environnement et De la Maîtrise de l'Energie ADEME, the Ministry of Higher Education and Research, Hauts de France Regional Council and European Regional Development Fund (ERDF) through the Contrat de Projets Etat Region (CPER CLIMIBIO). The authors also thank the Centre d'Etudes et de Recherches Lasers et Applications CERLA for technical help and financial support to this project. Finally, the authors would like to thank Dr. Miranda Lawson for her invaluable support.

## Author contributions

Jessy Elias, Pascal Demaux, Amaury Lahccen, and Benedicte Calimet carried out all the experiments. Luc-Sy Tran, Jeremy Bourgalais, Laurent Nahon, and Gustavo Garcia participated in the synchrotron experiments, the analysis of the data, and the writing of the publication. Alessandro Faccinetto and Xavier Mercier contributed equally in the supervision of this work, the analysis of the data and the writing of the publication.

## Competing interests

The authors declare no competing interests.

## Additional information

**Supplementary information** The online version contains supplementary material available at https://doi.org/10.1038/s42004-025-01689-7.

**Correspondence** and requests for materials should be addressed to X. Mercier.

**Peer review information** *Communications Chemistry* thanks Kim Cuong Le and the other, anonymous, reviewers for their contribution to the peer review of this work.